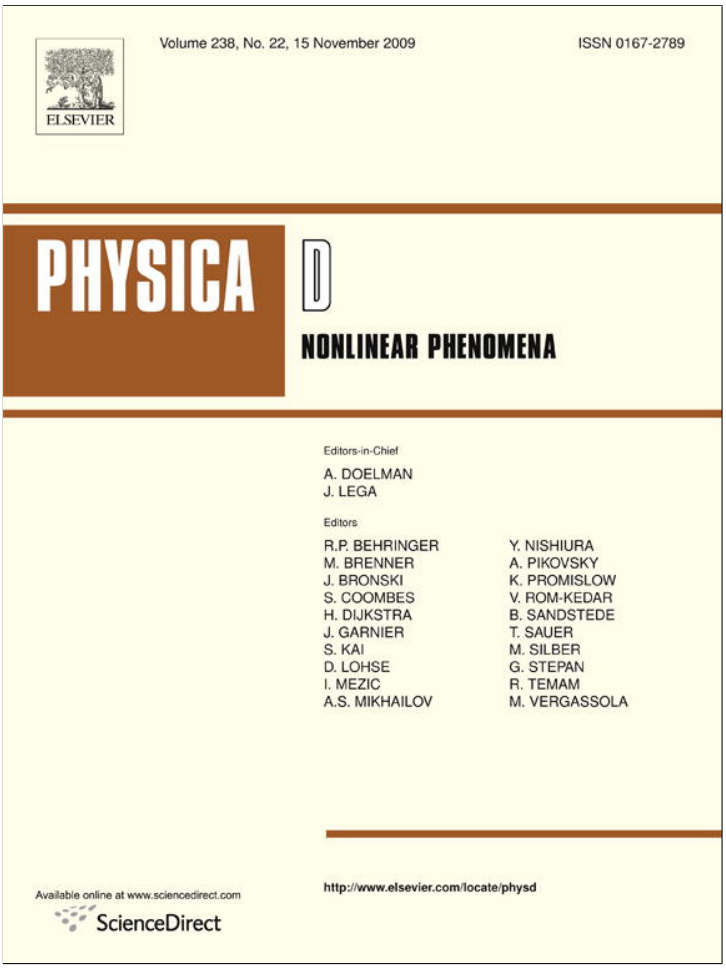

Physica D 238 (2009) 2216–2226

Contents lists available at ScienceDirect

Physica D

journal homepage: www.elsevier.com/locate/physd

Interlaced solitons and vortices in coupled DNLS lattices

J. Cuevas [a,*], Q.E. Hoq [b], H. Susanto [c], P.G. Kevrekidis [d]

[a] Grupo de Física No Lineal, Universidad de Sevilla. Departamento de Física Aplicada I. Escuela Universitaria Politécnica, C/ Virgen de África, 7, E-41011 Sevilla, Spain

[b] Department of Mathematics, Western New England College, Springfield, MA 01119, USA

[c] School of Mathematical Sciences, University of Nottingham, University Park, Nottingham, NG7 2RD, United Kingdom

[d] Department of Mathematics and Statistics, University of Massachusetts, Amherst, MA 01003-4515, USA

ARTICLE INFO

Article history:
Received 11 March 2009
Received in revised form
29 July 2009
Accepted 7 September 2009
Available online 15 September 2009
Communicated by S. Kai

Keywords:
Solitons
Discrete nonlinear Schrödinger equation
Manakov model
Vortices

ABSTRACT

In the present work, we propose a new set of coherent structures that arise in nonlinear dynamical lattices with more than one component, namely interlaced solitons. In the anti-continuum limit of uncoupled sites, these are waveforms whose one component has support where the other component does not. We illustrate systematically how one can combine dynamically stable unary patterns to create stable ones for the binary case of two-components. For the one-dimensional setting, we provide a detailed theoretical analysis of the existence and stability of these waveforms, while in higher dimensions, where such analytical computations are far more involved, we resort to corresponding numerical computations. Lastly, we perform direct numerical simulations to showcase how these structures break up, when they are exponentially or oscillatorily unstable, to structures with a smaller number of participating sites.

1. Introduction

One of the highly active areas in the investigation of Hamiltonian nonlinear systems over the past decade has been the examination of nonlinear dynamical lattices of the discrete nonlinear Schrödinger (DNLS) type. This development has arisen chiefly due to the multitude of applications of pertinent models that have emerged in areas such as nonlinear optics and atomic physics.

More specifically, in the optical context, the setting of fabricated AlGaAs waveguide arrays [1] has been one of the most prototypical ones for the application of DNLS models. There, the interplay of discreteness and nonlinearity revealed many interesting features including Peierls-Nabarro potential barriers, diffraction, diffraction management [2], and gap solitons [3], among others. More recently, higher dimensional phenomena such as two-dimensional discrete diffraction [4], and soliton formation [5] have been observed in square (but also in non-square [6]) femtosecond laser written waveguide arrays in fused silica; see also the reviews [7,8] and references therein.

Another recent development, which also promoted the analysis of discrete systems in connection with nonlinear optics was the proposal [9] and creation [10,11] of optically induced photonic lattices in photorefractive crystals such as SBN. This paved the way for the observation of a large set of exciting nonlinear wave-related phenomena in such crystals. As a representative subset, we mention here the formation of patterns such as dipole [12], quadrupole [13] and necklace [14] solitary waves, impurity modes [15], discrete vortices [16,17], rotary waves [18], higher order Bloch modes [19] and gap vortices [20], two-dimensional (2D) Bloch oscillations and Landau–Zener tunneling [21], wave formation in honeycomb [22], hexagonal [23] and quasi-crystalline lattices [24], and recently the study of Anderson localization in disordered photonic lattices [25]. Although this setting is mostly studied in the continuum context with a periodic potential (and sometimes in the presence of the inherent crystal anisotropy), it has also spurred a number of studies in the DNLS context with the saturable photorefractive nonlinearity [26,27].

A further physical realization of such nonlinear dynamical lattices arose over the past few years in atomic physics through the examination of Bose–Einstein condensates (BECs) trapped in periodic potentials. There, once again, a reduction of the relevant model can be formulated in the tight-binding approximation within the mean-field limit, reducing the so-called Gross–Pitaevskii equation with a periodic potential to a genuinely discrete nonlinear Schrödinger equation [28].

In both the nonlinear optical and in the atomic physics settings discussed above, multi-component systems were also examined in recent investigations. In particular, the first observations of discrete vector solitons in optical waveguide arrays were reported in [29], the emergence of multipole patterns in vector photorefractive crystals was presented in [30], while numerous experiments

* Corresponding author.
E-mail address: jcuevas@us.es (J. Cuevas).

0167-2789/$ – see front matter © 2009 Elsevier B.V. All rights reserved.
doi:10.1016/j.physd.2009.09.002

with BECs were directed towards studies of mixtures of different spin states of ^{87}Rb [31,32] or ^{23}Na [33] and even ones of different atomic species such as ^{41}K–^{87}Rb [34] and ^{7}Li–^{133}Cs [35]. It should be noted that while the above BEC experiments did not include the presence of an optical lattice, the addition of such an external optical potential is certainly feasible within the present experimental capabilities [36].

Our aim in the present work is to propose and analyze a family of solutions particular to multicomponent (in particular, binary) systems of DNLS equations, although generalizations to a higher number of components are certainly possible. We dub these proposed solutions "interlaced" discrete solitons and vortices. The name stems from the feature that the profiles of the modes in the two interacting components will have a vanishing intersection of excited sites in the extreme discrete limit of zero coupling between adjacent nodes of the lattice. In these structures, the first component will be excited where the second component is not and vice-versa. In the one-dimensional case, we show how to interlace in a stable fashion simple, as well as more elaborate, bound states of the system [37]. For such solutions, we consider their existence and stability properties also from an analytical point of view, using as a starting point the anti-continuum limit (of no-coupling between the sites). We then generalize our considerations to higher dimensional settings, showcasing the potentially stable interlacing of more elaborate structures, such as discrete vortices [38] (and also of vortices with non-vortical structures). We present detailed stability diagrams of such interlaced structures, and also examine their dynamics when they are found to be unstable.

Our presentation is structured as follows. In Section 2, we present the model and general mathematical setup. In Section 3, we illustrate both analytically and numerically the properties of such structures in 1d settings. In Section 4, we generalize these considerations to a numerical investigation of higher dimensional settings. Finally, in Section 5, we summarize our findings and present our conclusions.

2. Model equations and mathematical setup

We consider a set of coupled DNLS equations

$$\begin{aligned} &\mathrm{i}\dot{U}_n + (g_{11}|U_n|^2 + g_{12}|V_n|^2)U_n + C\Delta_D U_n = 0,\\ &\mathrm{i}\dot{V}_n + (g_{12}|U_n|^2 + g_{22}|V_n|^2)V_n + C\Delta_D V_n = 0, \end{aligned} \tag{1}$$

where n is a D-Dimensional index and Δ_D is the discrete Laplacian in D dimensions. We look for stationary solutions $\{u_n\}, \{v_n\}$ through the relations

$$U_n(t) = \exp(\mathrm{i}\Lambda_1 t)u_n, \qquad V_n(t) = \exp(\mathrm{i}\Lambda_2 t)v_n. \tag{2}$$

The dynamical equations (1) then transform into

$$\begin{aligned} &-\Lambda_1 u_n + (g_{11}|u_n|^2 + g_{12}|v_n|^2)u_n + C\Delta_D u_n = 0,\\ &-\Lambda_2 v_n + (g_{12}|u_n|^2 + g_{22}|v_n|^2)v_n + C\Delta_D v_n = 0. \end{aligned} \tag{3}$$

The stability is determined in a frame rotating with frequency Λ_1 for $U_n(t)$ and Λ_2 for $V_n(t)$, i.e., we suppose that

$$\begin{aligned} U_n(t) &= \exp(\mathrm{i}\Lambda_1 t)[u_n + \xi_n^{(1)}(t)],\\ V_n(t) &= \exp(\mathrm{i}\Lambda_2 t)[v_n + \xi_n^{(2)}(t)]. \end{aligned} \tag{4}$$

The small perturbations $\xi_n^{(k)}(t)$, with $k = 1, 2$, can be expressed as

$$\begin{aligned} \xi_n^{(1)}(t) &= a_n \exp(\mathrm{i}\lambda t) + b_n \exp(-\mathrm{i}\lambda^* t),\\ \xi_n^{(2)}(t) &= c_n \exp(\mathrm{i}\lambda t) + d_n \exp(-\mathrm{i}\lambda^* t), \end{aligned} \tag{5}$$

leading to the linear stability equations

$$\lambda J\overline{\xi_n} = M_n\overline{\xi_n} + C(\overline{\xi_{n+1}} + \overline{\xi_{n-1}}), \tag{6}$$

with

$$\overline{\xi_n} = (a_n \quad b_n^* \quad c_n \quad d_n^*)^{\mathrm{T}}, \qquad J = \begin{pmatrix} 1 & 0 & 0 & 0\\ 0 & -1 & 0 & 0\\ 0 & 0 & 1 & 0\\ 0 & 0 & 0 & -1 \end{pmatrix}, \tag{7}$$

$$M_n = \begin{pmatrix} K_{1,n} & g_{11}u_n^2 & g_{12}u_n v_n^* & g_{12}u_n v_n\\ g_{11}(u_n^2)^* & K_{1,n} & g_{12}u_n^* v_n^* & g_{12}u_n^* v_n\\ g_{12}u_n^* v_n & g_{12}u_n v_n & K_{2,n} & g_{22}v_n^2\\ g_{12}u_n^* v_n^* & g_{12}u_n v_n^* & g_{22}(v_n^2)^* & K_{2,n} \end{pmatrix}, \tag{8}$$

$$\begin{aligned} K_{1,n} &= -\Lambda + 2g_{11}|u_n|^2 + g_{12}|v_n|^2 - 2C,\\ K_{2,n} &= -\Lambda + 2g_{22}|v_n|^2 + g_{12}|u_n|^2 - 2C. \end{aligned}$$

Soliton and vortex solutions are calculated using methods based on the anti-continuous limit. Upon calculating these solutions at $C = 0$, we continue them to finite coupling by varying C for different values of the other parameters (such as the interspecies nonlinearity strength g_{12}).

We are interested in interlaced solitons (ISs) in 1D lattices and interlaced vortices (IVs) in 2D and 3D lattices. The excited sites at $C = 0$ have the freedom of a phase factor $\exp(\mathrm{i}\phi)$, while it should be noted that $u_n v_n = 0$ at the corresponding excited site (i.e., the two species are never excited on the same site for our interlaced waveforms). The values of the fields at the excited sites at the anti-continuous limit are:

$$\tilde{u} = \sqrt{\Lambda_1/g_{11}}, \qquad \tilde{v} = \sqrt{\Lambda_2/g_{22}}. \tag{9}$$

In what follows, we choose $\Lambda_1 = \Lambda_2 \equiv \Lambda$ and $g_{11} = g_{22} = 1$. We also choose $g_{12} \leq 1$ since for $g_{12} > 1$ interlaced solitons and vortices are unstable for every value of $C > 0$.

3. Analytical and numerical results for 1d interlaced solitons

3.1. Existence and stability

We consider interlaced solitons which are labeled by $|AB\rangle \equiv |A\rangle|B\rangle$, where $A, B = 0, 1, 2, \ldots$. This number indicates the "order" of the excited state at the anti-continuous limit, whose phase $\phi = 0, \pi$ is chosen so that the isolated solitons (i.e. when $g_{12} = 0$) are stable for any small C. For instance, the ground state $|0\rangle$ means $u_n = \tilde{u}\delta_{n,0}$ and the first excited state $|1\rangle$ will be taken to mean $u_n = \tilde{u}(\delta_{n,1} - \delta_{n,-1})$ at the AC limit. Thus, the state $|01\rangle$ corresponds to $u_n = \tilde{u}\delta_{n,0}$, $v_n = \tilde{v}(\delta_{n,1} - \delta_{n,-1})$ and $|12\rangle$ to $u_n = \tilde{u}(\delta_{n,1} - \delta_{n,-1})$, $v_n = \tilde{v}(\delta_{n,2} + \delta_{n,-2}) - \delta_{n,0}$.

We first analyze the $|01\rangle$ state, which is stable for $C < C_0$. At $C = C_0$ the ISs become unstable through Hopf bifurcations (the value of C_0 differs as a function of the rest of the system parameters such as g_{12}, however the above scenario is robust). Cascades of these types of bifurcations arise as C increases and, when, $C \geq C_1$, the ISs become also exponentially unstable. There is a special region for $g_{12} \in [0.27, 0.37]$ where the system experiences an inverse Hopf bifurcation recovering the stability in a window. The system becomes unstable again through Hopf bifurcations for $g_{12} \in [0.27, 0.34]$ and exponential instabilities for $g_{12} \in [0.35, 0.37]$. Besides, for $g_{12} \in [0.38, 0.47]$ there exist windows with only exponential instabilities. Fig. 1 illustrates all of the above features, by showcasing a typical example of the $|01\rangle$ state, a typical continuation of its principal linearization eigenfrequencies λ, and a full two-parameter diagram of the stability of this state in the two-parameter plane (C, g_{12}).

For $|12\rangle$ states, the scenario is essentially similar to the $|01\rangle$ case, although, in practice, it is considerably simpler due to the absence of any inverse Hopf bifurcations and restabilization windows. Fig. 2 shows the corresponding features for $|12\rangle$, similarly to Fig. 1 for the $|01\rangle$ case.

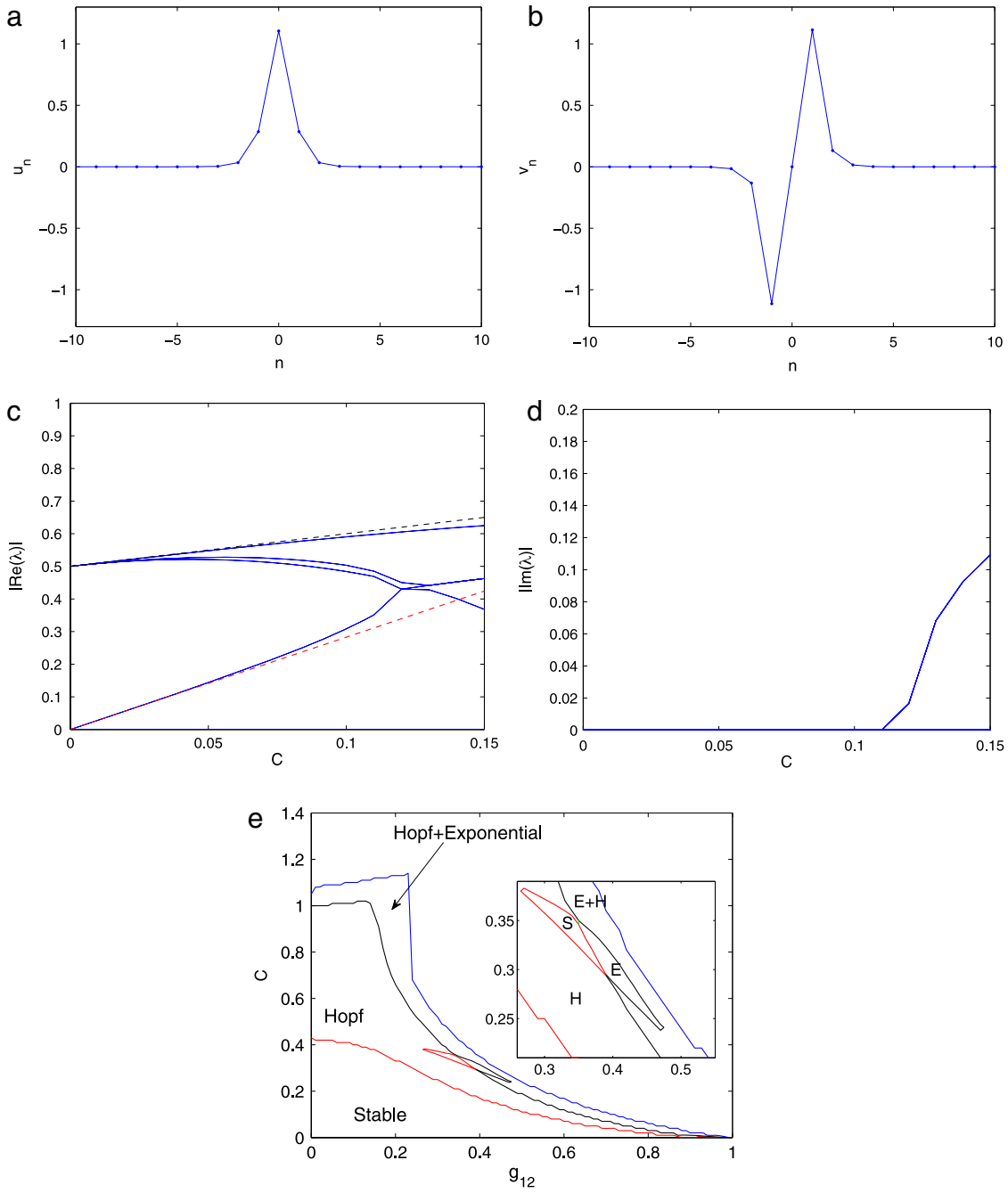

Fig. 1. (a–b) Profiles of $|01\rangle$ interlaced solitons with $g_{12} = 0.5$ and $C = 0.15$. (c–d) Dependence on C of the real and imaginary parts of eigenfrequencies of small perturbations about $|01\rangle$ with $g_{12} = 0.5$. Dashed lines correspond to the analytical predictions of Eqs. (17) and (18). (e) Two-parameter stability diagram in the plane of intersite (C) and inter-component (g_{12}) coupling, indicating regions of occurrence of Hopf bifurcations (H), exponential instability (E), and the domain of stability (S).

3.2. Dynamics of unstable solitons

First, we analyze the dynamics of $|01\rangle$ ISs. Fig. 3 shows the evolution of a typically unstable (i.e. oscillatory unstable) $|01\rangle$ IS with $g_{12} = 0.2$ and $C = 0.6$. The oscillatory evolution of the instability eventually transforms the mode into a $|00\rangle$ state, which is a stable state of the system. The final excited site is typically the same for the $\{U_n\}$ and $\{V_n\}$ coordinates, although in some cases, the asymptotic excited site is not necessarily the same. However, the amplitude of the nth site is not identical, i.e. $|u_n| \neq |v_n|$. In a similar vein, Fig. 4 shows the evolution of an oscillatorily unstable $|12\rangle$ IS with $g_{12} = 0.2$ and $C = 0.4$, and, analogously to the $|01\rangle$ case, the IS evolves to a $|00\rangle$ state (although the finally populated site is not the central one of the original configuration).

Some insight into the evolution can be established from an energy analysis of the different stationary solutions coexisting with the same norm for a given value of C and g_{12}. The energy is given by:

$$H = \sum_n \frac{C}{2}(|u_{n+1} - u_n|^2 + |v_{n+1} - v_n|^2) - \frac{g_{11}}{2}|u_n|^4 - g_{12}|u_n|^2|v_n|^2 - \frac{g_{22}}{2}|v_i|^4. \quad (10)$$

Fig. 3(c) shows the energy of $|00\rangle$ and $|01\rangle$ states versus C. The $|00\rangle$ states have been calculated fixing the norm of each component and enforcing that it is the same as that of the corresponding $|01\rangle$ states. It is observed that $|00\rangle$ states are always more energetically favorable than $|01\rangle$. A similar analysis can be performed for

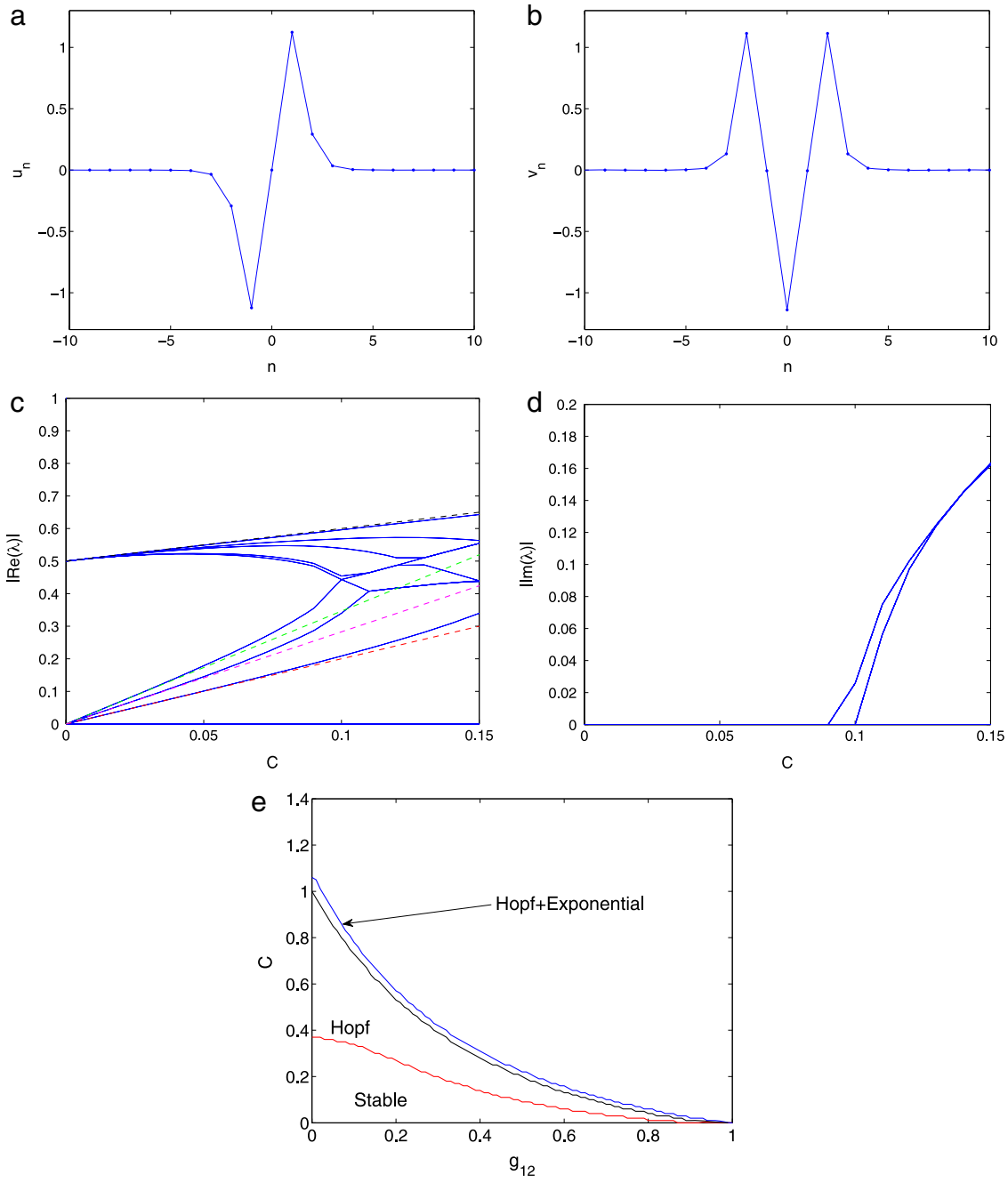

Fig. 2. (a–b) Profiles and (c–d) dependence on C of the real and imaginary parts of eigenfrequencies of small perturbations of $|12\rangle$ showing the same features and for the same parameters as in Fig. 1. Dashed lines correspond to the theoretical predictions of Eqs. (20) and (18). (e) Two-parameter stability diagram in the plane of the intersite (C) and inter-component (g_{12}) coupling.

$|12\rangle$ states. It shows that the energy for $|12\rangle$ is higher than that of, in turn, $|01\rangle$ and $|00\rangle$ states, justifying the dynamical evolution of Figs. 3 and 4.

3.3. Perturbation analysis

In this subsection, we attempt to understand in some more detail the above observed results of the numerical computations in connection with the stability properties of the interlaced soliton solutions. More specifically, we evaluate explicit expressions of the interlaced solitons' eigenvalues for the configurations discussed above. The method is based on the expansion in the coupling constant C in the vicinity of the anti-continuum limit.

In the limit of $C = 0$, as illustrated above, there are two types of solutions, i.e. $u_n = v_n = 0$, and the non-zero solutions given by Eqs. (9). In this limit, one can also easily notice that the eigenvalue problem (6) will give

$$\lambda = \pm\Lambda, \pm\Lambda(1 - g_{12}/g_{11}), \pm\Lambda(1 - g_{12}/g_{22}) \tag{11}$$

for the zero solutions and

$$\lambda = \pm 0 \tag{12}$$

for the non-zero solutions (9).

It can be directly inferred from the analysis of the underlying linear problem that the stable eigenvalues $\lambda = \pm\Lambda$ will expand creating a band of continuous spectrum when C is increased.

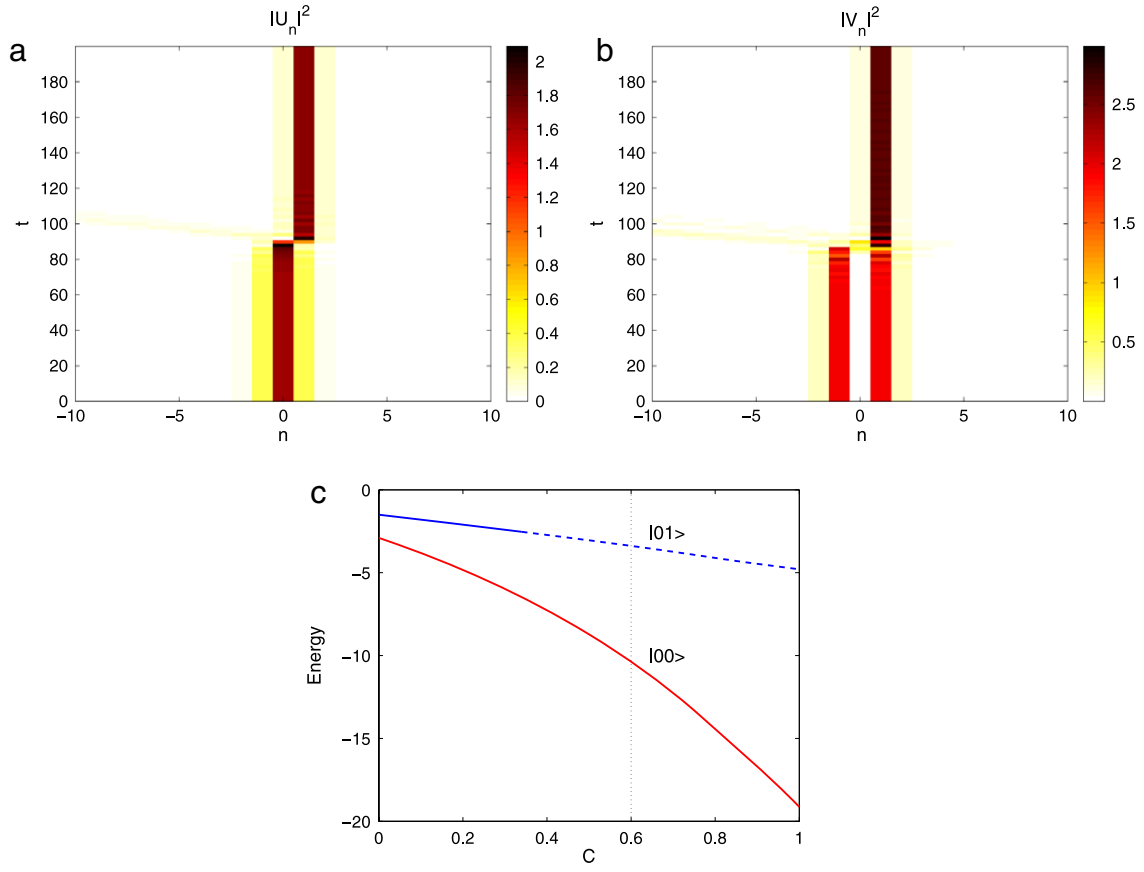

Fig. 3. (a) and (b) Time evolution of the density of the two components for a slightly perturbed unstable $|01\rangle$ IS with $g_{12} = 0.2$ and $C = 0.6$. (c) Energy dependence with respect to C of $|01\rangle$ and $|00\rangle$ states. For a given value of C, the $|00\rangle$ state has the same norm as the $|01\rangle$ state. The dashed line represents the unstable solitons.

Therefore, this eigenvalue will not be discussed further. The instability for a soliton solution will then be determined by the bifurcation of the remaining eigenvalues.

Let us now first consider the profile of $|01\rangle$ ISs. It is clear that for finite C the solutions will be deformed from their AC-limit profile. The solution up to $O(C)$ is then found to be

$$u_0 = \sqrt{\frac{\Lambda}{g_{11}}} + \frac{C}{\sqrt{\Lambda g_{11}}}, \qquad u_1 = u_{-1} = \frac{C}{\sqrt{\Lambda g_{11}(1 - g_{12}/g_{22})}}, \tag{13}$$
$$v_0 = 0, \qquad v_1 = -v_{-1} = \sqrt{\frac{\Lambda}{g_{22}}} + \frac{C}{\sqrt{\Lambda g_{22}}}.$$

The next step is to consider the stability problem when the coupling is turned on. To leading order, the eigenvalue problem of this particular configuration is given by

$$\mathcal{M}\Xi = \lambda\sigma\Xi, \tag{14}$$

where

$$\sigma = \mathrm{diag}(J), \qquad \Xi = \begin{pmatrix} \xi_{-2} \\ \xi_{-1} \\ \xi_0 \\ \xi_1 \\ \xi_2 \end{pmatrix}, \tag{15}$$

$$\mathcal{M} = \begin{pmatrix} M_{-2} & CId_{4\times4} & 0 & 0 & 0 \\ CId_{4\times4} & M_{-1} & CId_{4\times4} & 0 & 0 \\ 0 & CId_{4\times4} & M_0 & CId_{4\times4} & 0 \\ 0 & 0 & CId_{4\times4} & M_1 & CId_{4\times4} \\ 0 & 0 & 0 & CId_{4\times4} & M_2 \end{pmatrix}, \tag{16}$$

and $Id_{4\times4}$ is the identity matrix of size 4×4.

Since we have expanded u_n and v_n in a power series of C, then it is natural that we also expand all the involved quantities in C. Performing a regular perturbation analysis to each order in C of the eigenvalue problem (14) (see the Appendix), one can show that for the stability of (13) there is a pair of eigenvalues bifurcating from zero given by

$$\lambda = \pm 2C\sqrt{\frac{g_{11}}{g_{11} - g_{12}}} + \mathcal{O}(C^2), \tag{17}$$

and two pairs of eigenvalues

$$\lambda = \pm(1 - g_{12}/g_{22})(\Lambda + 2C), \pm(1 - g_{12}/g_{11})(\Lambda + 2C). \tag{18}$$

The same procedure can also be similarly and immediately applied to the configuration $|12\rangle$ ISs. The only difference is that for that solution one will obtain a stability matrix $\mathcal{M}$ of size 28×28.

For $|12\rangle$ISs, we can obtain the solution in a power series of C as

$$u_0 = 0, \qquad u_1 = -u_{-1} = \sqrt{\frac{\Lambda}{g_{11}}} + \frac{C}{\sqrt{\Lambda g_{11}}},$$
$$u_2 = -u_{-2} = \frac{C}{\sqrt{\Lambda g_{11}}(1 - g_{12}/g_{22})}, \tag{19}$$
$$v_0 = -v_2 = -v_{-2} = -\sqrt{\frac{\Lambda}{g_{22}}} - \frac{C}{\sqrt{\Lambda g_{22}}}, \qquad v_1 = v_{-1} = 0.$$

Continuing the search for eigenvalues, we will also immediately obtain eigenvalues of (19) bifurcating from zero as

$$\lambda = \pm\sqrt{\frac{2}{1 - g_{12}/g_{11}}}C, \pm\sqrt{\frac{6}{1 - g_{12}/g_{11}}}C, \pm\sqrt{\frac{4}{1 - g_{12}/g_{22}}}C. \tag{20}$$

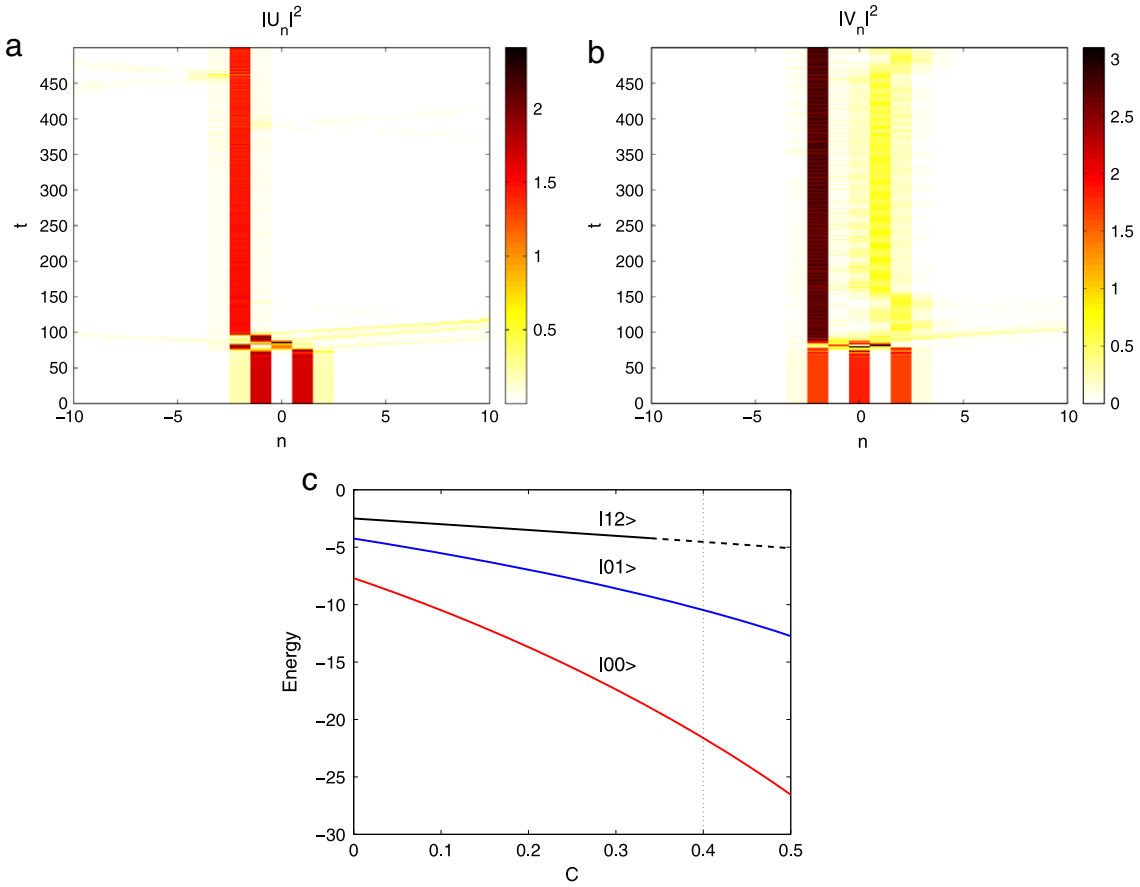

Fig. 4. (a) and (b) Time evolution of the density of the two components for a slightly perturbed unstable $|12\rangle$ IS with $g_{12} = 0.2$ and $C = 0.4$. (c) Energy dependence with respect to C of $|12\rangle$, $|01\rangle$ and $|00\rangle$ states. For a given value of C, the $|01\rangle$ and $|00\rangle$ states have the same norm as the $|12\rangle$ state. The dashed line represents the unstable solitons.

Bifurcations from the non-zero eigenvalues for this case can also be shown to yield Eq. (18).

The above analytical expressions give us a detailed handle on the dependence of the relevant eigenvalues on the system parameters. Comparisons of the analytical results obtained here with the numerical ones are presented in Figs. 1 and 2 where one can see that the analytical expressions are in fairly good agreement with the numerical results. It should be noted that although such analytical considerations are procedurally straightforward to generalize in higher dimensions, the relevant calculations are extremely tedious and will thus not be pursued here. Instead, we now turn to numerical computations to showcase the existence and potential stability of interlaced solitons and vortices in higher-dimensional settings.

4. Numerical results for interlaced structures in higher dimensions

For the case of 2D lattices, we consider two different interlaced structures. On the one hand, we examine interlaced vortices (IVs) whose configurations in the AC limit are given by $u_{0,1} = \tilde{u}, u_{0,-1} = -\tilde{u}, u_{1,0} = \mathrm{i}\tilde{u}, u_{-1,0} = -\mathrm{i}\tilde{u}$; $v_{1,1} = -\mathrm{i}\tilde{v}, v_{1,-1} = \tilde{v}, v_{-1,-1} = \mathrm{i}\tilde{v}, v_{-1,1} = -\tilde{v}$. On the other hand, we also study a discrete soliton interlaced with a vortex (IVSs) whose configurations in the AC limit are given by $u_{0,1} = \tilde{u}, u_{0,-1} = -\tilde{u}, u_{1,0} = \mathrm{i}\tilde{u}, u_{-1,0} = -\mathrm{i}\tilde{u}, v_{0,0} = \tilde{v}$.

IVs experience a set of bifurcation scenaria which are qualitatively similar to those of the $|12\rangle$ ISs. The structures are stable for low values of the coupling and for $g_{12} < 1$. For larger values of C (or respectively g_{12}) they destabilize due to a Hamiltonian Hopf bifurcation, while further increase of the relevant parameters will induce a mixture of both Hopf and exponential instabilities, as shown in Fig. 5. IVSs experience the same basic bifurcation phenomena, with the principal difference that they appear to exist for all values of C (within the range examined i.e., up to $C = 2$) for $g_{12} \leq 0.4$. Also, notably, the IVSs experience solely Hopf bifurcations in a fairly small region inside the exponential+Hopf region. Figs. 5 and 6 summarize the corresponding findings in a way similar to that of the 1d configurations, presenting not only typical profiles of the modes, but also typical mono-parametric continuations, as well as their full two-parameter stability diagram in the space of inter-site and inter-species coupling. An important conclusion of the figures, that it is relevant to highlight, is that both interlaced vortices and interlaced soliton-vortex bound states may be stable for sufficiently small coupling and interspecies interaction strength.

In the case of 3D lattices, we consider two interlaced vortices conjoined in the shape of a cube. In the AC limit, this cube is given by $u_{-1,1,1} = \tilde{u}, u_{1,-1,1} = -\tilde{u}, u_{-1,-1-1} = i\tilde{u}, u_{1,1,-1} = -i\tilde{u}$; $v_{1,-1,-1} = \tilde{v}, v_{-1,1,-1} = -\tilde{v}, v_{1,1,1} = i\tilde{v}, v_{-1,-1,1} = -i\tilde{v}$. The structure is stable near the AC limit, with the size of the window of stability diminishing as g_{12} approaches 1, and with instability setting in via Hopf bifurcations. In the 2-parameter continuation results shown in Fig. 7, the coupling is only continued to $C = 0.75$, but it is observed that for values between $g_{12} \approx 0.703$ and $g_{12} = 1$, the instability further degenerates into Hopf and exponential instabilities. It should also be noted that within the region of instability, there exist isolated points or very narrow regions where inverse Hopf bifurcations may be observed, which have been omitted from the graph for clarity. Let us note in passing here that the interlaced vortices in the "vortex cube" shown in Fig. 7 are perhaps not the prototypical interlaced structure that one would expect in 3D; instead one might expect a structure where

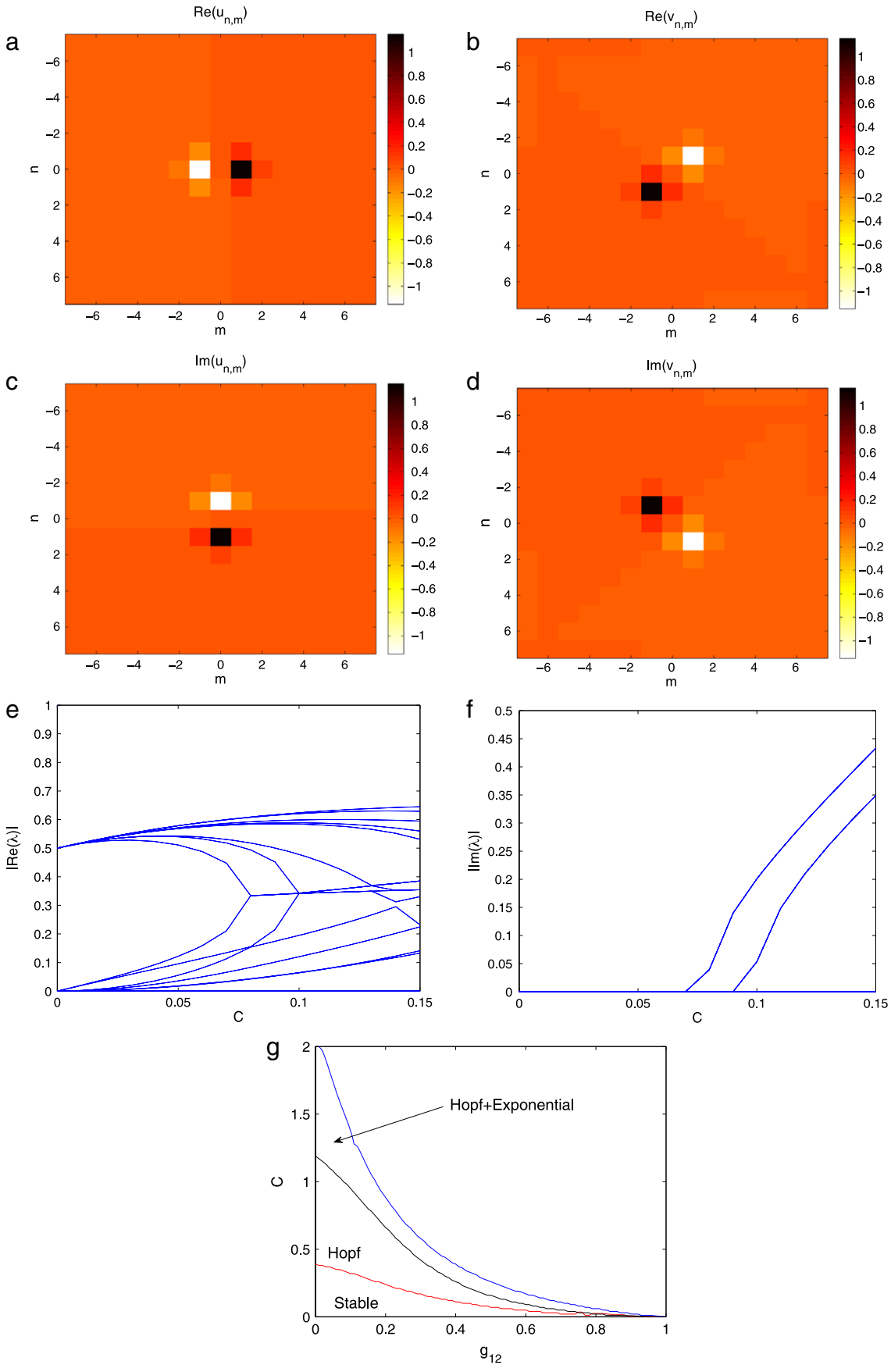

Fig. 5. (a–d) Plot of real and imaginary parts of interlaced vortices with $g_{12} = 0.5$ and $C = 0.1$. (e–f) Dependence on C of the real and imaginary parts of eigenfrequencies of small perturbations about such solutions with $g_{12} = 0.5$. (g) Two-parameter stability diagram in the plane of intersite (C) and inter-component (g_{12}) coupling.

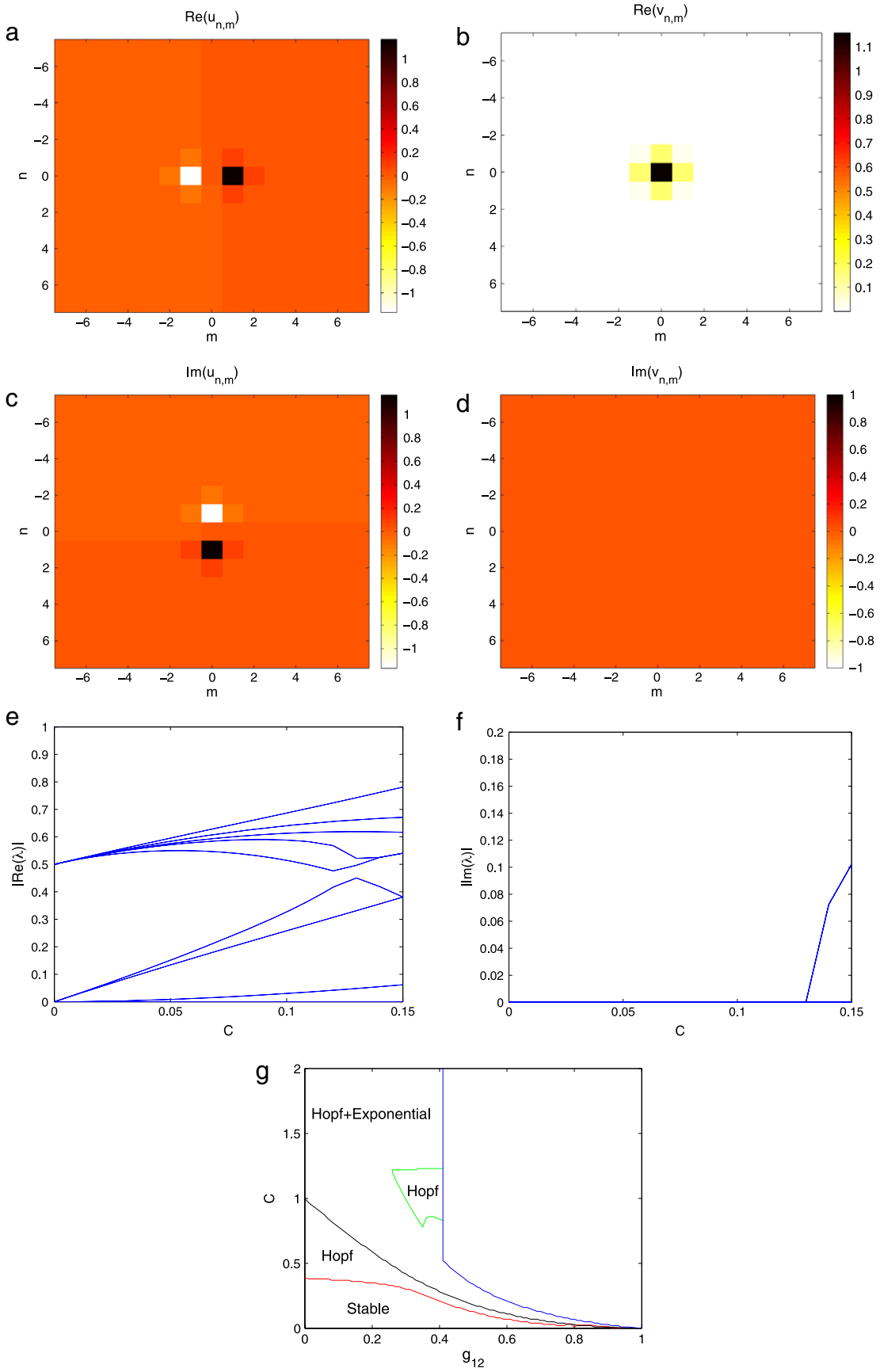

Fig. 6. (a–d) Plot of real and imaginary parts and (e–f) dependence on C of the real and imaginary parts of eigenfrequencies of small perturbations about interlaced soliton-vortex solutions, showing the same features and for the same parameters as in Fig. 5. (g) The corresponding two-parameter stability diagram.

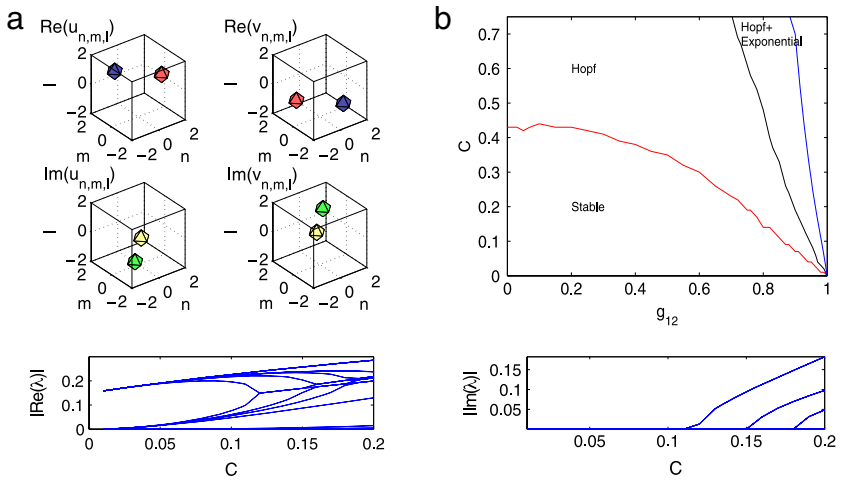

Fig. 7. (a) The top set of four panels shows an interlaced cube ($g_{12} = 0.85$) in a grid of size $11 \times 11 \times 11$ that has been continued to coupling $C = 0.20$. The level contours shown correspond to $\mathrm{Re}(u_{n,m,l}) = \mathrm{Re}(v_{n,m,l}) = \pm 0.5 \max\{u_{n,m,l}\}$, in blue and red (dark gray and gray, in the black-and-white version) respectively, while the imaginary ones, $\mathrm{Im}(u_{n,m,l}) = \mathrm{Im}(v_{n,m,l}) = \pm 0.5 \max\{u_{n,m,l}\}$, are shown by green and yellow (light and very light gray, in the black-and-white version) respectively. The bottom panel shows the real eigenfrequencies of small perturbation. (b) The top panel shows the stability diagram, while the bottom panel shows the imaginary eigenfrequencies of small perturbations.

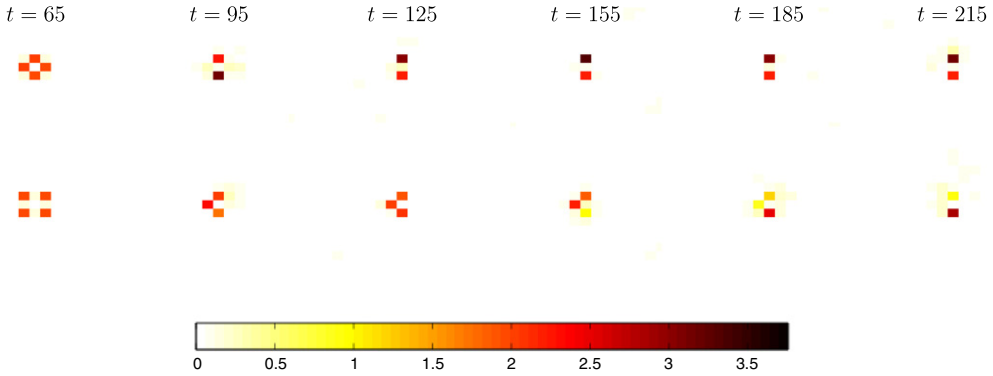

Fig. 8. Snapshots showing (top) $|U_n(t)|^2$ and (bottom) $|V_n(t)|^2$ for unstable IVs with $g_{12} = 0.2$ and $C = 0.3$.

each vortex is confined in a diagonal plane within the cube (with the two such planes intersecting transversally). We were, however, unable to trace such a structure even in the vicinity of the anti-continuum limit.

4.1. Dynamics of unstable structures

The dynamics of the oscillatorily unstable IVs in 2D lattices with $g_{12} = 0.2$ and $C = 0.3$ is shown in Fig. 8. The evolution results in the transformation of the original structure into single-peaked or multi-peaked solitons. Excited peaks do not coincide for U_n and V_n. The vorticity is lost in the process (recall that the vorticity needn't be conserved in the case of the lattice). Fig. 9 shows the dynamics of an oscillatorily unstable interlaced vortex-soliton structure with $g_{12} = 0.2$ and $C = 0.45$. This mode evolves spontaneously towards single-peaked solitons. The excited peaks are on the same site in both lattices in this example.

The dynamics of the interlaced cube with $g_{12} = 0.85$ is shown in Fig. 10. Here the coupling is continued to $C = 0.6$. This is well past the threshold of stability for this value of g_{12}, and takes the configuration into the region of both exponential and oscillatory instabilites. It is observed that when a peturbation of magnitude 0.01 is applied, only a single site survives for long times (in this case for the V field).

Although these are prototypical results of the dynamical evolution, which we have generically observed to lead to less elaborate (and often purely single-peaked) structures in this setting, it should be stressed that the specific details of the unstable dynamical evolution of each structure depend considerably on the values of the parameters, as well as partially on the type/strength of the perturbation.

5. Conclusions and future challenges

In the present work, we have illustrated the possibility of successfully interlacing structures which are stable in each one of the components (either simple ones, such as single site solitary waves, or more elaborate ones, such as bound states and vortices) in order to produce stable multi-component interlaced solitons/vortices. We have continued the resulting structures from the anti-continuum limit of no inter-site coupling to finite coupling and illustrated the intervals of stability, as well as the ones of both exponential and oscillatory (Hopf) instabilities. We have given detailed two-parameter diagrams of the stable ranges of the solutions as a function of the inter-site and inter-component couplings. These revealed that the linear stability of the interlaced structures necessitates sufficiently weak coupling (typically no larger than 0.4, with the relevant range decreasing as the inter-component interaction is increased) and sufficiently weak inter-component interaction (i.e., $g_{12} < 1$). It can naturally be assumed that the instability of interlaced states for $g_{12} > 1$ can be attributed to the destabilizing effect of strong nonlinear attraction between the two components. Finally, we examined the dynamical evolution of the

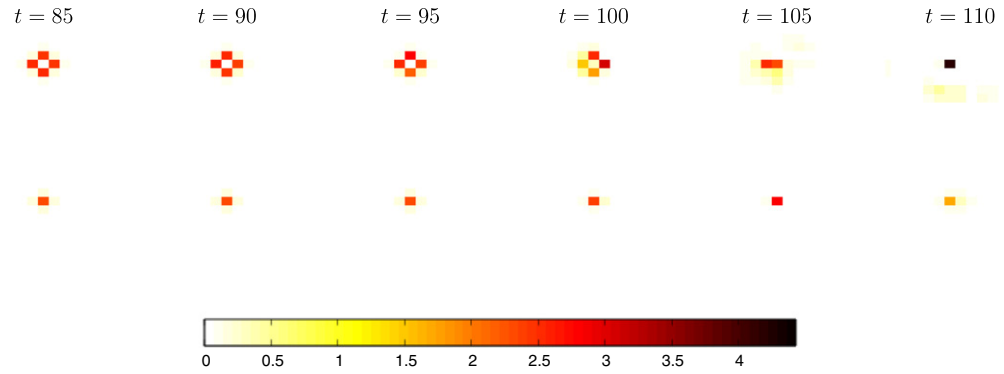

Fig. 9. Snapshots showing (top) $|U_n(t)|^2$ and (bottom) $|V_n(t)|^2$ for unstable interlaced vortex-solitons with $g_{12} = 0.2$ and $C = 0.45$.

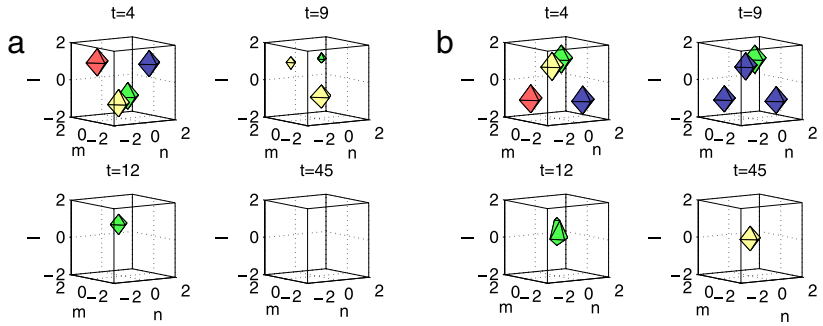

Fig. 10. Snapshots showing evolution of the two fields (a and b, respectively) for the interlaced cube with $g_{12} = 0.85$ in a grid of size $11 \times 11 \times 11$ where the coupling has been continued to $C = 0.6$. All iso-contour plots are defined as $\mathrm{Re}(u_{n,m,l}) = \mathrm{Re}(v_{n,m,l}) = \pm 0.75 = \mathrm{Im}(u_{n,m,l}) = \mathrm{Im}(v_{n,m,l})$, where in the figure, dark gray (blue) and gray (red) colors pertain to iso-contours of the real part of the solutions, while the light gray (green) and very light gray (yellow) colors correspond to the iso-contours of the imaginary part. The configuration was pertubed by a random noise of amplitude 0.01 in order to expedite the onset of the instability.

instability of such interlaced structures, which typically resulted in the destruction of the waveforms, in favor of simpler, more stable dynamical patterns.

Nevertheless, there is still a number of important open questions for future consideration. For instance, it would be particularly interesting to examine whether it would be possible for the inter-component coupling to actually stabilize structures that are dynamically unstable in the single-component setting. Also, it would be useful to possess a systematic classification of the solutions (interlaced and non-interlaced ones) available in the multi-component system setting, similarly to the one-component classifications of [37,38]. Such efforts are currently underway and will be reported in future publications.

Appendix. Analytical calculations of the eigenvalues of 1D interlaced solitons

Here we will discuss in more detail the analytical calculations we performed to calculate the eigenvalues of $|01\rangle$ ISs and $|12\rangle$ ISs presented above.

To solve the eigenvalue problem (14) perturbatively for the eigenvalues of (13), we start by writing $\mathcal{M} = \mathcal{M}_0 + C\mathcal{M}_1 + C^2\mathcal{M}_2 + \mathcal{O}(C^3)$, $\Xi = \Xi_0 + C\Xi_1 + C^2\Xi_2 + \mathcal{O}(C^3)$ and $\lambda = \lambda_0 + C\lambda_1 + C^2\lambda_2 + \mathcal{O}(C^3)$. It can be checked that $\mathcal{M}_0$ is a singular self-adjoint matrix.

Substituting the expansions to the eigenvalue problem will give us to the leading order

$$\mathcal{M}_0\Xi_0 = \lambda_0\sigma\Xi_0, \tag{A.1}$$

from which one will obtain that λ_0 is given by Eqs. (11) and (12). In the following, let us first consider the case of $\lambda_0 = 0$ which are of three pairs, with the corresponding eigenvalues of $\mathcal{M}_0\Xi_0 = 0$ denoted by e_j, $j = 1, 2, 3$. Therefore, one can write

$$\Xi_0 = \sum_{j=1}^{3} c_j e_j.$$

The next order equation of (14) gives us

$$\mathcal{M}_0\Xi_1 = \lambda_1\sigma\Xi_0 - \mathcal{M}_1\Xi_0. \tag{A.2}$$

Using the Fredholm alternative theorem, the above equation will have a solution if the right hand side is orthogonal to the null space of $\mathcal{M}_0$, which it is. Hence, the value of the correction λ_1 cannot be obtained yet and a solution Ξ_1 of (A.2) can therefore be calculated for *any* λ_1.

The equation of order $\mathcal{O}(C^2)$ from (6) can be easily deduced to be

$$\mathcal{M}_0\Xi_2 = \lambda_2\sigma\Xi_0 + \lambda_1\sigma\Xi_1 - \mathcal{M}_1\Xi_1 - \mathcal{M}_2\Xi_0. \tag{A.3}$$

Projecting the equation above to e_j, $j = 1, 2, 3$, i.e. basis of the null space of $\mathcal{M}_0$, will give us the following eigenvalue matrix

$$\begin{pmatrix} \frac{-2g_{11}}{(g_{11}-g_{12})\Lambda} & 0 & \frac{-2g_{11}}{(g_{11}-g_{12})\Lambda} \\ 0 & 0 & 0 \\ \frac{-2g_{11}}{(g_{11}-g_{12})\Lambda} & 0 & \frac{-2g_{11}}{(g_{11}-g_{12})\Lambda} \end{pmatrix} \begin{pmatrix} c_1 \\ c_2 \\ c_3 \end{pmatrix} = -\frac{\lambda_1^2}{\Lambda} \begin{pmatrix} c_1 \\ c_2 \\ c_3 \end{pmatrix}, \tag{A.4}$$

which can be immediately solved to yield

$$\lambda_1 = \pm 0, \pm 0, \pm 2\sqrt{\frac{g_{11}}{g_{11}-g_{12}}}. \tag{A.5}$$

This illustrates that there is a pair of eigenvalues bifurcating from zero given by (17) above.

The same procedure can be applied to bifurcations of the non-zero eigenvalues. In this case, the calculation is even simpler as applying the Fredholm alternative to the $\mathcal{O}(C)$ equation of (14) already gives us a solvability condition from which we obtain the bifurcating eigenvalues (18).

For the stability of $|12\rangle$ ISs, one can perform the same analysis as above. Following the same procedures, one will obtain that for

$$\begin{pmatrix} \frac{-2g_{11}}{(g_{11}-g_{12})\Lambda} & 0 & \frac{-2g_{11}}{(g_{11}-g_{12})\Lambda} & 0 & 0 \\ 0 & \frac{-2g_{22}}{(g_{22}-g_{12})\Lambda} & 0 & \frac{-2g_{22}}{(g_{22}-g_{12})\Lambda} & 0 \\ \frac{-2g_{11}}{(g_{11}-g_{12})\Lambda} & 0 & \frac{-4g_{11}}{(g_{11}-g_{12})\Lambda} & 0 & \frac{-2g_{11}}{(g_{11}-g_{12})\Lambda} \\ 0 & \frac{-2g_{22}}{(g_{22}-g_{12})\Lambda} & 0 & \frac{-2g_{22}}{(g_{22}-g_{12})\Lambda} & 0 \\ 0 & 0 & \frac{-2g_{11}}{(g_{11}-g_{12})\Lambda} & 0 & \frac{-2g_{11}}{(g_{11}-g_{12})\Lambda} \end{pmatrix} \begin{pmatrix} c_1 \\ c_2 \\ c_3 \\ c_4 \\ c_5 \end{pmatrix} = -\frac{\lambda_1^2}{\Lambda} \begin{pmatrix} c_1 \\ c_2 \\ c_3 \\ c_4 \\ c_5 \end{pmatrix}$$

Box I.

the profile (19) the reduced eigenvalue matrix is given, in place of (A.4), by the equation given in Box I, which finally yields (20).

Bifurcations of the non-zero eigenvalues of the configuration (19) can be calculated similarly to the case of $|01\rangle$ ISs above from which one will also obtain the same expression as (18).

References

[1] H.S. Eisenberg, Y. Silberberg, R. Morandotti, A.R. Boyd, J.S. Aitchison, Phys. Rev. Lett. 81 (1998) 3383.
[2] R. Morandotti, U. Peschel, J.S. Aitchison, H.S. Eisenberg, Y. Silberberg, Phys. Rev. Lett. 83 (1999) 2726–2729;
H.S. Eisenberg, Y. Silberberg, R. Morandotti, J.S. Aitchison, Phys. Rev. Lett. 85 (2000) 1863.
[3] D. Mandelik, R. Morandotti, J.S. Aitchison, Y. Silberberg, Phys. Rev. Lett. 92 (2004) 093904.
[4] T. Pertsch, U. Peschel, F. Lederer, J. Burghoff, M. Will, S. Nolte, A. Tünnermann, Opt. Lett. 29 (2004) 468.
[5] A. Szameit, J. Burghoff, T. Pertsch, S. Nolte, A. Tünnermann, F. Lederer, Opt. Express 14 (2006) 6055.
[6] A. Szameit, D. Blomer, J. Burghoff, T. Pertsch, S. Nolte, A. Tünnermann, Appl. Phys. B 82 (2006) 507.
[7] D.N. Christodoulides, F. Lederer, Y. Silberberg, Nature 424 (2003) 817–823;
A.A. Sukhorukov, Yu.S. Kivshar, H.S. Eisenberg, Y. Silberberg, IEEE J. Quantum Electron 39 (2003) 31;
F. Lederer, G.I. Stegeman, D.N. Christodoulides, G. Assanto, M. Segev, Y. Silberberg, Phys. Rep. 463 (2008) 1.
[8] S. Aubry, Physica 103D (1997) 201;
S. Flach, C.R. Willis, Phys. Rep. 295 (1998) 181.
[9] N.K. Efremidis, S. Sears, D.N. Christodoulides, J.W. Fleischer, M. Segev, Phys. Rev. E 66 (2002) 046602.
[10] J.W. Fleischer, M. Segev, N.K. Efremidis, D.N. Christodoulides, Nature 422 (2003) 147.
[11] J.W. Fleischer, T. Carmon, M. Segev, N.K. Efremidis, D.N. Christodoulides, Phys. Rev. Lett. 90 (2003) 023902.
[12] J. Yang, I. Makasyuk, A. Bezryadina, Z. Chen, Opt. Lett. 29 (2004) 1662.
[13] J. Yang, I. Makasyuk, A. Bezryadina, Z. Chen, Stud. Appl. Math. 113 (2004) 389.
[14] J. Yang, I. Makasyuk, P.G. Kevrekidis, H. Martin, B.A. Malomed, D.J. Frantzeskakis, Z. Chen, Phys. Rev. Lett. 94 (2005) 113902.
[15] F. Fedele, J. Yang, Z. Chen, Opt. Lett. 30 (2005) 1506.
[16] D.N. Neshev, T.J. Alexander, E.A. Ostrovskaya, Yu.S. Kivshar, H. Martin, I. Makasyuk, Z. Chen, Phys. Rev. Lett. 92 (2004) 123903.
[17] J.W. Fleischer, G. Bartal, O. Cohen, O. Manela, M. Segev, J. Hudock, D.N. Christodoulides, Phys. Rev. Lett. 92 (2004) 123904.
[18] Y.V. Kartashov, V.A. Vysloukh, L. Torner, Phys. Rev. Lett. 93 (2004) 093904;
X. Wang, Z. Chen, P.G. Kevrekidis, Phys. Rev. Lett. 96 (2006) 083904.
[19] D. Träger, R. Fischer, D.N. Neshev, A.A. Sukhorukov, C. Denz, W. Królikowski, Yu.S. Kivshar, Opt. Express 14 (2006) 1913.
[20] G. Bartal, O. Manela, O. Cohen, J.W. Fleischer, M. Segev, Phys. Rev. Lett. 95 (2005) 053904.
[21] H. Trompeter, W. Królikowski, D.N. Neshev, A.S. Desyatnikov, A.A. Sukhorukov, Yu.S. Kivshar, T. Pertsch, U. Peschel, F. Lederer, Phys. Rev. Lett. 96 (2006) 053903.
[22] O. Peleg, G. Bartal, B. Freedman, O. Manela, M. Segev, D.N. Christodoulides, Phys. Rev. Lett. 98 (2007) 103901.
[23] C.R. Rosberg, D.N. Neshev, A.A. Sukhorukov, W. Krolikowski, Yu.S. Kivshar, Opt. Lett. 32 (2007) 397.
[24] B. Freedman, G. Bartal, M. Segev, R. Lifshitz, D.N. Christodoulides, J.W. Fleischer, Nature 440 (2006) 1166.
[25] T. Schwartz, G. Bartal, S. Fishman, M. Segev, Nature 446 (2007) 52.
[26] L. Hadzievski, A. Maluckov, M. Stepić, D. Kip, Phys. Rev. Lett. 93 (2004) 033901;
L. Hadzievski, A. Maluckov, M. Stepić, Opt. Express 15 (2007) 5687.
[27] E.P. Fitrakis, P.G. Kevrekidis, H. Susanto, D.J. Frantzeskakis, Phys. Rev. E 75 (2007) 066608;
V.M. Rothos, H.E. Nistazakis, P.G. Kevrekidis, D.J. Frantzeskakis, J. Phys. A 42 (2009) 025207.
[28] P.G. Kevrekidis, D.J. Frantzeskakis, R. Carretero-González (Eds.), Emergent Nonlinear Phenomena in Bose–Einstein Condensates: Theory and Experiment, Springer-Verlag, Heidelberg, 2008.
[29] J. Meier, J. Hudock, D. Christodoulides, G. Stegeman, Y. Silberberg, R. Morandotti, J.S. Aitchison, Phys. Rev. Lett. 91 (2003) 143907.
[30] Z. Chen, J. Yang, A. Bezryadina, I. Makasyuk, Opt. Lett. 29 (2004) 1656.
[31] C.J. Myatt, E.A. Burt, R.W. Ghrist, E.A. Cornell, C.E. Wieman, Phys. Rev. Lett. 78 (1997) 586.
[32] K.M. Mertes, J.W. Merrill, R. Carretero-González, D.J. Frantzeskakis, P.G. Kevrekidis, D.S. Hall, Phys. Rev. Lett. 99 (2007) 190402.
[33] D.M. Stamper-Kurn, M.R. Andrews, A.P. Chikkatur, S. Inouye, H.-J. Miesner, J. Stenger, W. Ketterle, Phys. Rev. Lett. 80 (1998) 2027.
[34] G. Modugno, G. Ferrari, G. Roati, R.J. Brecha, A. Simoni, M. Inguscio, Science 294 (2001) 1320.
[35] M. Mudrich, S. Kraft, K. Singer, R. Grimm, A. Mosk, M. Weidemüller, Phys. Rev. Lett. 88 (2002) 253001.
[36] O. Morsch, E. Arimondo, in: T. Dauxois, S. Ruffo, E. Arimondo, M. Wilkens (Eds.), Dynamics and Thermodynamics of Systems with Long-range Interactions, Springer, Berlin, 2002, pp. 312–331.
[37] G.L. Alfimov, V.A. Brazhnyi, V.V. Konotop, Physica D 194 (2004) 127;
D.E. Pelinovsky, P.G. Kevrekidis, D.J. Frantzeskakis, Physica D 212 (2005) 1.
[38] D.E. Pelinovsky, P.G. Kevrekidis, D.J. Frantzeskakis, Physica D 212 (2005) 20;
M. Lukas, D.E. Pelinovsky, P.G. Kevrekidis, Physica D 237 (2008) 339.